Supplemental materials for: Selective collective emission from a dense atomic ensemble coupled to a nanophotonic resonator

Xinchao Zhou,[1] Deepak A. Suresh,[1] F. Robicheaux,[1,2] and Chen-Lung Hung[1,2,*]

[1] *Department of Physics and Astronomy, Purdue University, West Lafayette, IN 47907, USA*
[2] *Purdue Quantum Science and Engineering Institute, Purdue University, West Lafayette, IN 47907, USA*

(Dated: June 28, 2025)

I. Theoretical model

Here we briefly discuss important steps for modeling collective emission dynamics of the system. Detailed description of the theoretical model can be found in Ref. [S1]. We consider weak driving in the bad cavity limit. After adiabatically eliminating the cavity field, the evolution of the system can be described by a set of coupled equations for N atomic dipoles [S2, S3],

$$\frac{d\sigma^i}{dt} = i\Delta_a\sigma^i + i\Omega_i - i\sum_{i,j}^{N}(J_{ij} - i\frac{\Gamma_{ij}}{2})\sigma^j \tag{S1}$$

where $\sigma^i = \langle\sigma^i_{ge}\rangle$ is the expectation value of the operator $\sigma_{ge} \equiv |g\rangle\langle e|$ acting on the i-th atom, $\Delta_a = \omega_p - \omega_a$ is the detuning of the laser frequency ω_p from the transition frequency ω_a, Ω_i is the position-dependent driving amplitude for the i-th atom, $J_{ij} = J_{\mathrm{dd}}(\mathbf{r}_i, \mathbf{r}_j)$ and $\Gamma_{ij} = \Gamma_{\mathrm{dd}}(\mathbf{r}_i, \mathbf{r}_j)$ represent the coherent and dissipative parts of the resonant dipole-dipole interaction mediated by the cavity and the non-guided modes. See Sec. IV for further discussions.

The coupled dipole equations can be written using a vector notation as

$$\dot{\vec{\sigma}} = i\mathbf{M}\vec{\sigma} + i\vec{\Omega}\,, \tag{S2}$$

where $\vec{\sigma} = \{\sigma^1, \ldots, \sigma^N\}$, $\vec{\Omega} = \{\Omega_1, \ldots, \Omega_N\}$ and $\mathbf{M}$ is an $N \times N$ coupling matrix depicting photon-mediated dipole-dipole interactions via a single-mode running-wave cavity (i.e. the whispering-gallery mode) and the non-guided free space modes. The coupling matrix consists of the summation of these contributions and the full expression can be found in Ref. [S1].

As discussed in the main text, the coupling matrix $\mathbf{M}$ can be diagonalized with N eigenvectors $\vec{v}_\xi$ of complex eigenvalues λ_ξ. We can decompose any given initial state as $\vec{\sigma}_0 = \sum_{\xi=1}^{N} w_\xi \vec{v}_\xi$, where w_ξ is the amplitude of each eigenvector. For the steady state (SS) created by a long excitation pulse, we have $\vec{\sigma}_0 = -\mathbf{M}^{-1}\vec{\Omega}$. For the timed-Dicke state (TDS) created by a short excitation pulse, $\vec{\sigma}_0 \propto \vec{\Omega}$.

We study the evolution of the system after switching off the excitation pulse at $t = 0$. The ensuing dynamics of the atomic dipoles then follows the equation $\dot{\vec{\sigma}} = i\mathbf{M}\vec{\sigma}$. The solution can be written as

$$\vec{\sigma}(t) = \sum_{\xi=1}^{N} w_\xi e^{i\lambda_\xi t}\vec{v}_\xi\,, \tag{S3}$$

* clhung@purdue.edu

where w_ξ is the amplitude of the eigenvectors in $\vec{\sigma}(0) = \vec{\sigma}_0$.

Due to the complex eigenvalues, where $\Gamma_\xi = 2\mathrm{Im}[\lambda_\xi] > 0$ for all ξ, the collective atomic excitation will decay down to the ground state and a photon is emitted. With the conservation of energy, the photon emission rate R can be evaluated through the population de-excitation rate,

$$R(t) = -\frac{d(\vec{\sigma}^\dagger \vec{\sigma})}{dt} = \vec{\sigma}^\dagger (i\mathbf{M}^\dagger - i\mathbf{M})\vec{\sigma}\,. \tag{S4}$$

Since the coupling matrix $\mathbf{M}$ contains the cavity and the non-guided mode contributions, we could split the total emission rate into two parts,

$$R(t) = R_c(t) + R_f(t)\,, \tag{S5}$$

where $R_c(t)$ represents the photon emission rate to the cavity mode (i.e. the collection channel) and $R_f(t)$ the emission rate into the non-guided modes (i.e. the free space).

Given an initial atomic state $\vec{\sigma}_0$, we can fully calculate the photon emission rate into each channel. We note that, if only one eigenstate is excited initially ($\vec{\sigma}_0 = \vec{v}_\xi$), $R_c(t)$ and $R_f(t)$ decay single-exponentially with a single decay rate Γ_ξ. However, given a random atomic distribution in an atomic ensemble, many eigenstates can be excited with non-zero amplitudes $w_\xi \neq 0$ for $\xi \in [1, \ldots, N]$. Photon emission rates into the collection channel $R_c(t)$ and the free space $R_f(t)$ can display much more complex decay dynamics [S4, S5].

In Fig. S1, we show the calculated photon emission rates $R_c(t)$ and $R_f(t)$ of 10 sample atomic configurations drawn from an experimentally measured density distribution [S6] together with the ensemble-averaged emission curves which are the same as those of Fig. 2 in the main text. Instead of decaying monotonically, the photon emission rates display oscillatory behaviors due to coherent interactions between the atomic dipoles. These oscillatory features are averaged out in ensemble averaging.

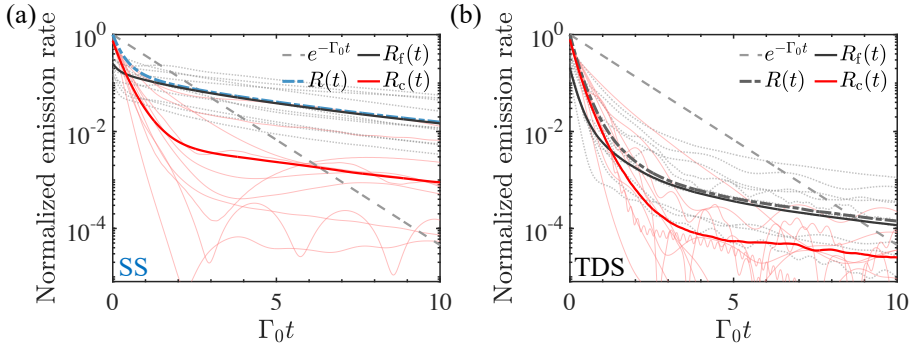

FIG. S1. Time evolution of ensemble-averaged photon emission rates, $R_c(t)$ (thick red curves) and $R_f(t)$ (thick black curves), of (a) the SS and (b) the TDS, respectively. In both plots, thin curves are photon emission rates, of sample atomic configurations, into the whispering-gallery mode (red solid lines) and free space (gray dotted lines), respectively. Dash-dotted curves mark the total emission rates $R(t)$. Dashed lines mark single atom decay.

II. Decay rate measurement and experimental data analysis

We excite the system through the bus waveguide, as shown in Fig. 1 in the main text, and record the photon counts through the output port. We send weak resonant pulses with a width of approximately 200 ns to drive the system into the SS and monitor the photon emission after the excitation pulse is extinguished, as shown in Fig. S2. The pulse is repeated every 600 ns for 2 ms in each experimental cycle and the same experiment is repeated for 2000 times. For measurements with the TDS, the width of the excitation pulse is approximately 6 ns, as shown in the inset of Fig. S2(d), and the pulse is repeated every 200 ns for 2ms. We extract the decay rate Γ_{exp} by fitting the averaged photon emission curve with $I = I_0 e^{-\Gamma_{\mathrm{exp}} t} + b$, where b is a fit parameter for the background. We obtain the error bars of Γ_{exp} in Fig. 3 by choosing different initial times (gray bands in Fig. S2) to perform fitting.

We confirm theoretically that the short pulses can approximately drive the TDS. In Fig. S3(a), we show the calculated excited mode amplitudes, which match with those of the ideal state reasonably well. In Fig. S3(b), the calculated decay rates $\Gamma_{\mathrm{th}} = -\dot{R}_c/R_c$ in the limit of $C_1 \to 0$ also shows nearly identical atom number dependence.

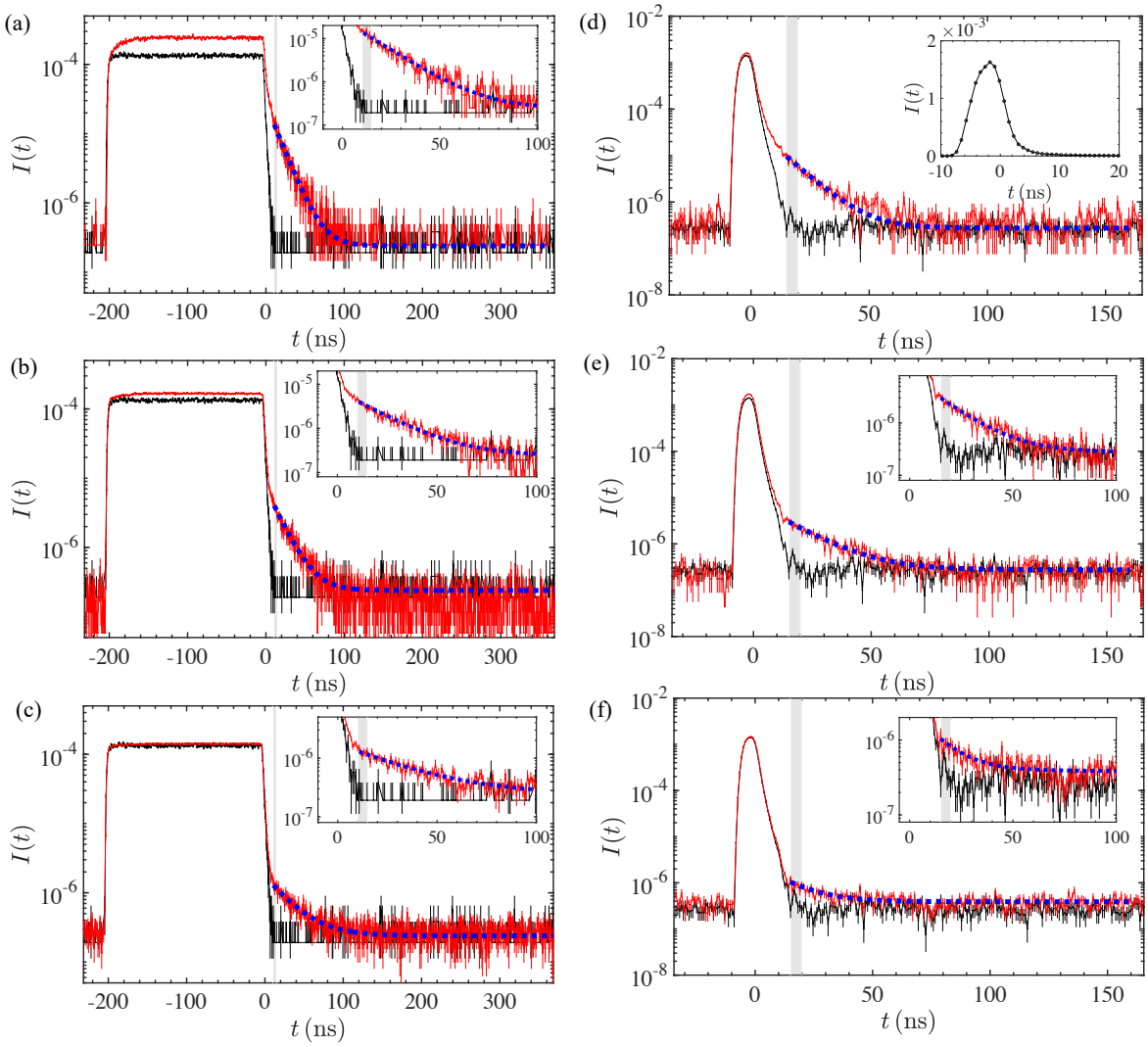

FIG. S2. Resonant pulses for driving the system into (a-b) the steady state and (c-d) the timed-Dicke state, with (red lines) and without atoms (black lines). The photon counts $I(t)$ are recorded with time bins of 0.8 ns resolution. After the excitation pulse is extinguished (marked by left edge of the shaded region), the averaged photon counts are fitted to extract the decay rate $\Gamma_{\rm exp}$. The insets in (a-c) and (e-f) show the zoom-in figures and the blue-dashed lines show the fitted exponential curves $I = I_0 e^{-\Gamma_{\rm exp} t} + b$. Inset in (c) shows the averaged pulse with 6 ns full width at half maximum (FWHM) to excite the timed-Dicke state. (a-c) Measurements for the steady state with atom number $N = 58 \pm 8$ but different $C_1 = 0.022$ (a), 0.006 (b) and 0.0023 (c), respectively. The fitted $\Gamma_{\rm exp}$ in (a-c) are $(2.38 \pm 0.13,\ 1.60 \pm 0.05,\ 0.97 \pm 0.02)\Gamma_0$, respectively. (d-f) Measurements for timed-Dicke state with atom number $N = 46 \pm 5$ and different $C_1 = 0.035$ (d), 0.008 (e) and 0.004 (f), respectively. The fitted $\Gamma_{\rm exp}$ in (d-f) are $(3.29 \pm 0.08,\ 1.99 \pm 0.08,\ 1.96 \pm 0.14)\Gamma_0$, respectively. The error bars of photon counts indicate the error of the mean.

In Fig. 4(b), we observe increasing decay rate $\Gamma^0_{\rm exp}$ (in the limit of $C_1 \to 0$) versus the atom number N for the TDS. Although this behavior is consistent with theoretical predictions [see also Fig. S3(b)], discrepancy is found in the magnitude. We cannot fully reconcile the discrepancy using the parameters estimated within our experimental uncertainties [S6]. We have varied several parameters in the numerical calculations, including the time dependence of excitation, the number of trapped atoms, and the variation of averaged single atom cooperativity C_1. We have tested that the 6 ns pulse duration does not alter the decay rate noticeably. However, we do note that significantly increasing the atom number N (by more than three-fold) while simultaneously reducing the value of C_1 could lead to a calculate decay rate approaching the measured value without affecting other experiment conclusions. To fully reconcile this discrepancy requires further investigations.

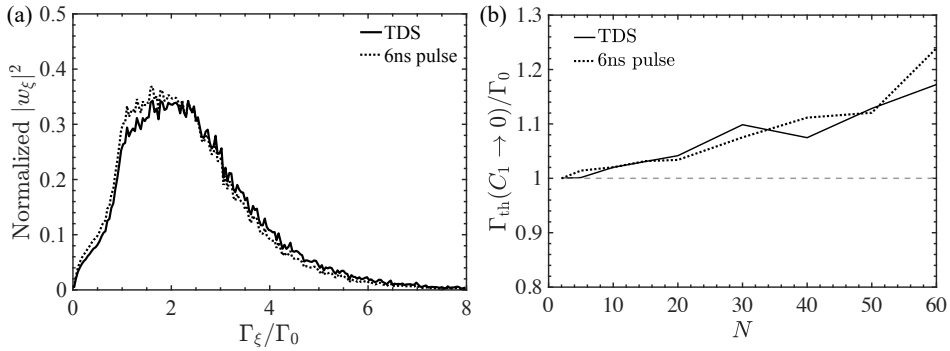

FIG. S3. (a) Normalized eigenstate population $|w_\xi|^2$ as a function of decay rate Γ_ξ for the timed-Dicke state (TDS) and the excitation prepared by a short pulse (6 ns FWHM) in the experiment. The distribution is sampled using 40000 random configurations of N = 50 atoms in the trap [S6] with an averaged single-atom cooperativity $C_1 = 0.05$. (b) Calculated decay rates $\Gamma_{\rm th}$ at $C_1 \to 0$ showing nearly identical atom number scaling in the two cases.

III. θ factor – ratio of the decay rate into different channels

As discussed in the main text, our measurement of $\Gamma_{\rm exp}$ is related to the time evolution of photon emission rates as

$$\Gamma_{\rm exp} \approx -\frac{\dot{R}_c}{R_c} = \Gamma_c + \Gamma_f \theta \,, \tag{S6}$$

where $\Gamma_c = -\dot{R}_c/R$ and $\Gamma_f = -\dot{R}_f/R$. The θ factor takes the ratio between the decay rates of R_c and R_f,

$$\theta = \frac{\dot{R}_c}{R_c} \times \frac{R_f}{\dot{R}_f} \,. \tag{S7}$$

Given that photon emission into free space is not monitored in the experiment, we numerically evaluate the θ factor for the SS and the TDS, respectively, and make use of this calculation to extract the decay rates Γ_c and Γ_f from the measured $\Gamma_{\rm exp}$ [Fig. 4(c-d)]. From theoretical calculations, we note that both $\dot{R}_c/R_c$ and $\dot{R}_f/R_f$ remain nearly constant in the early time from $t = 0$ to $1/\Gamma_0$, where Γ_0 is the single atom decay rate in free space. It suffices to show θ calculated at $t = 0$.

Figure S4 (a, c) show the θ factor as a function of the atom number N and the single-atom cooperativity parameter C_1. We find $\theta > 1$ for the SS, which is in clear distinction from $\theta \lesssim 1$ for the TDS. This suggests that, in the early time dynamics, the decay of emission rate R_f is slower than (comparable or faster than) that of R_c for the SS (TDS). This dynamics can be seen in the ensemble-averaged curves in Fig. S1.

In Fig. S4 (b, d), we plot the calculated $\Gamma_f\theta$. Within the experimental parameter range ($N \lesssim 60$ and $C_1 < 0.05$), the variation of $\Gamma_f\theta$ with respect to C_1 is generally small (roughly within 10% difference under a fixed atom number N). Hence, we extract $\Gamma_c = \Gamma_{\rm exp} - \Gamma^0_{\rm exp}$ in Fig. 4(d) by assuming that $\Gamma_f\theta$ is a constant and $\Gamma^0_{\rm exp} \approx \Gamma_f\theta$, where $\Gamma^0_{\rm exp}$ is the value of $\Gamma_{\rm exp}$ at $C_1 \to 0$ [Fig. 4(a)].

IV. Numerically calculated resonant dipole-dipole interaction

In the present theoretical analyses [S1], we adopt the Green's function formalism to evaluate the resonant dipole-dipole interactions. We include the cavity contribution to the total Green's function based on the calculated mode profile and the measured cavity linewidth. On the other hand, we adopt the analytical free space Green's tensor as an approximation for the non-guided mode contributions. We justify this approximation by noting that our measurements are primarily performed with trapped atoms localized at $z \gtrsim \lambda_0/2$ above the dielectric surfaces, where $\lambda_0 = 852$ nm is the transition wavelength in free space. At such a distance, surface-scattering modification to the free space Green's function is insignificant.

To verify this assumption, we perform finite-difference time domain (FDTD) calculations [S7] to compare the Green's functions in the presence or absence of a dielectric structure. We construct a point dipole source above a linear waveguide, without forming a cavity, and compute the dyadic Green's function $\mathbf{G}(\mathbf{r}_0, \mathbf{r}, \omega_0)$ to obtain the non-guided mode contribution (guided mode contribution is much smaller without the cavity enhancement). Here,

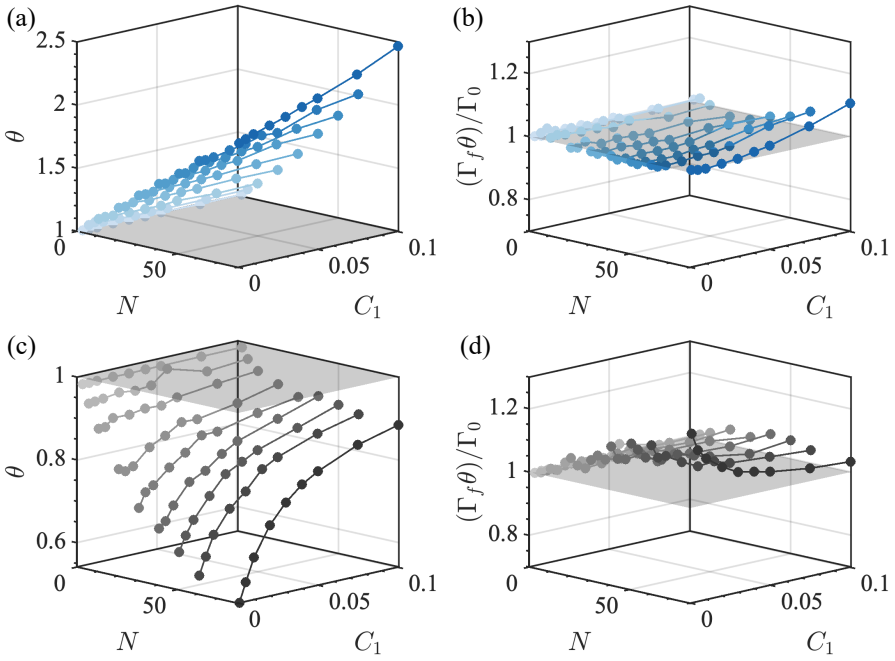

FIG. S4. θ factor for the SS (a) and the TDS (c) as function of C_1 and N. Shaded plane marks $\theta = 1$. (b, d) $\Gamma_f\theta$ for the SS (b) and the TDS (d), repectively.

ω_0 is the transition frequency, $\mathbf{r}_0$ is the location of the point dipole, and $\mathbf{r}$ is a position in space. We calculate the resonant dipole-dipole interaction using

$$J_{\rm dd}(\mathbf{r}) - i\frac{\Gamma_{\rm dd}(\mathbf{r})}{2} = -\frac{\mu_0\omega_0^2}{\hbar}\mathbf{d}^\dagger \cdot \mathbf{G}(\mathbf{r}_0, \mathbf{r}, \omega_0) \cdot \mathbf{d}\,, \tag{S8}$$

where μ_0 is the vacuum permeability, $\hbar$ is the reduced Planck constant, and $\mathbf{d}$ is the transition dipole moment. The real part of the dipole-dipole interaction $J_{\rm dd}$ is responsible for the collective energy shifts while the imaginary part $\Gamma_{\rm dd}$ could lead to collective dissipation dynamics such as superradiance and subradiance studied in this work.

In the FDTD calculations, the simulated Si_3N_4 waveguide is 326 nm thick and 950 nm wide, sitting on a dielectric slab formed by stacked SiO_2 (2.04 μm thick) and Si_3N_4 (583 nm thick) layers similar to the one used in the experiment. The waveguide extends along the y-axis for 10 μm until it enters the absorbing boundary layers. The point source is located at $\mathbf{r}_0 = (0, 0, 400)$ nm and the top surface of the waveguide is centered at the origin.

We compute $J_{\rm dd}$ and $\Gamma_{\rm dd}$ using Eq. (S8) for atomic dipoles polarized along the x-axis, which is transverse to the waveguide. The results are plotted in Fig. S5 and are compared with the values evaluated without any dielectric structure. Overall, the modification is small. Within the range $|\mathbf{r} - \mathbf{r}_0| \lesssim \lambda_0$, there is on-average $\sim 7\%$ difference in the dissipative rate $\Gamma_{\rm dd}$, and $\sim 12\%$ difference in the dispersive shift $J_{\rm dd}$. Given the diminishing differences at even larger $z_0 > 400$ nm, we conclude that using the analytical Green's function in free space to model the dipole-dipole interactions is a reasonable approximation.

[S1] D. A. Suresh, X. Zhou, C.-L. Hung, and F. Robicheaux, Collective emission and selective-radiance in atomic clouds and arrays coupled to a microring resonator, arXiv:2503.21121 (2025).

[S2] A. Asenjo-Garcia, M. Moreno-Cardoner, A. Albrecht, H. J. Kimble, and D. E. Chang, Exponential improvement in photon storage fidelities using subradiance and "selective radiance" in atomic arrays, Phys. Rev. X **7**, 031024 (2017).

[S3] R. T. Sutherland and F. Robicheaux, Collective dipole-dipole interactions in an atomic array, Phys. Rev. A **94**, 013847 (2016).

[S4] J. Kumlin, S. Hofferberth, and H. P. Büchler, Emergent universal dynamics for an atomic cloud coupled to an optical waveguide, Phys. Rev. Lett. **121**, 013601 (2018).

[S5] R. Pennetta, D. Lechner, M. Blaha, A. Rauschenbeutel, P. Schneeweiss, and J. Volz, Observation of coherent coupling between super- and subradiant states of an ensemble of cold atoms collectively coupled to a single propagating optical mode, Phys. Rev. Lett. **128**, 203601 (2022).

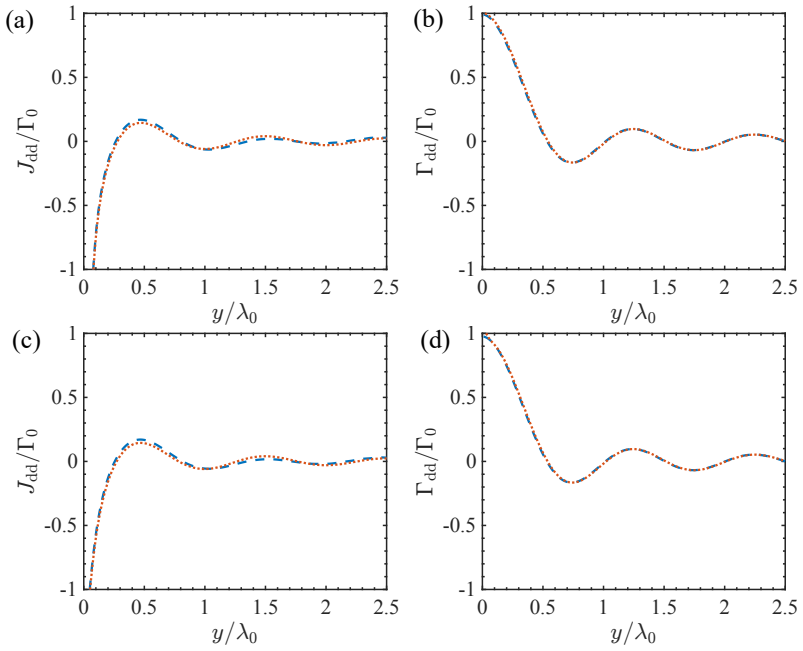

FIG. S5. Real and imaginary parts of the resonant dipole-dipole interactions, $J_{\rm dd}$ and $\Gamma_{\rm dd}$, evaluated in the presence (dashed curves) or absence (dotted curves) of the dielectric structure for (a-b) $\mathbf{r} = (0, y, 400\ \text{nm})$ and (c-d) $\mathbf{r} = (0, y, 350\ \text{nm})$, respectively. The point dipole source is located at $\mathbf{r}_0 = (0, 0, 400\ \text{nm})$.

[S6] X. Zhou, H. Tamura, T.-H. Chang, and C.-L. Hung, Trapped atoms and superradiance on an integrated nanophotonic microring circuit, Phys. Rev. X **14**, 031004 (2024).

[S7] A. F. Oskooi, D. Roundy, M. Ibanescu, P. Bermel, J. Joannopoulos, and S. G. Johnson, Meep: A flexible free-software package for electromagnetic simulations by the fdtd method, Computer Physics Communications **181**, 687 (2010).